A Compact Skin-Shear Device using a Lead-Screw Mechanism*

Pratheev Sreetharan, Ali Israr, and Priyanshu Agarwal

***Abstract*— We present a skin-shear actuator based on the lead screw mechanism. The lead screw mechanism is simple, reliable, offers fewer components, and accommodates into compact form-factors. We show mechanical design of a single assembly unit and implement multiple units in a single handheld device. We evaluate the actuator in one instrumentation-based test and one preliminary user study. Tests show that the actuator performance matches with the open-loop control scheme when no load is placed on the actuator. The performance deteriorates with loading, particularly when quicker and high amplitude stroke are required. The user study shows that information throughput with the skin-shear is comparable to vibrations through three digits on the hand. It is shown that small compact actuators (~5g) with efficient mechanisms can render displacements (>3mm) and forces (>1N) for easily differentiating skin-shear cues.**

I. Introduction

Wearable and handheld devices have evolved in the last decade to incorporate rich interactions in augmented and virtual reality applications. These devices are embedded with haptic feedback technologies to enhance physical interactions with the virtual content. Most commonly, vibrotactile actuators are incorporated due to their simple design, compact form-factor, small size, lightweight and low power requirements, and used for rendering simple object detection and manipulation feedback, such as tactile contacts, button clicks and surface texture. These actuators are driven by direct drives of a magnet and a coil and generate the desired motion without the need of a mechanical transmission [1].

Recently, researchers have incorporated clever designs of mechanisms and linkages on rotational electric motors to produce low-bandwidth and directional motion on skin-stretch and skin-indentation devices [2-4]. These skin devices render high fidelity dynamics of virtual objects and produced sensations that are comparable to those of stiffness, inertia and squeeze [3-5]. In these devices, high rotational shaft speed is reduced by gear-like transmission drives and translated into linear motion using pulley-cable, rack-pinion, scotch-yoke or crank-piston drives, etc. [6-9]. These transmissions usually have high efficiency; however, they require considerable space, generate undesirable audible noise and several small components in these transmissions may increase chances of failure and complexity in manufacturing and assembly.

In this paper, we investigate and present the design of a skin-shear device that is based on a lead-screw mechanism to convert rotational speed of a motor to the linear motion of a carriage in contact with the skin. Lead screws are common in consumer devices and used for high precision motion in disk drives and digital cameras. Lead-screws are advantageous in that the high rotational speed of a motor is directly converted into linear motion with desired force output, without the need of an intermediate transmission mechanism to step-down the motor speed. This reduction in number of components and complexity in design is specifically attractive for our application where multiple such skin-shear actuators need to be encapsulated in a wearable or handheld form-factor (Figure 1c). The lead screw designs have low efficiency, however, advanced design of leadscrews such as ball screws, magnetic lead screws, and folded leadscrews have shown to reduce noise and friction issues and achieve efficiencies greater than 60% and up to 95% [10, 11].

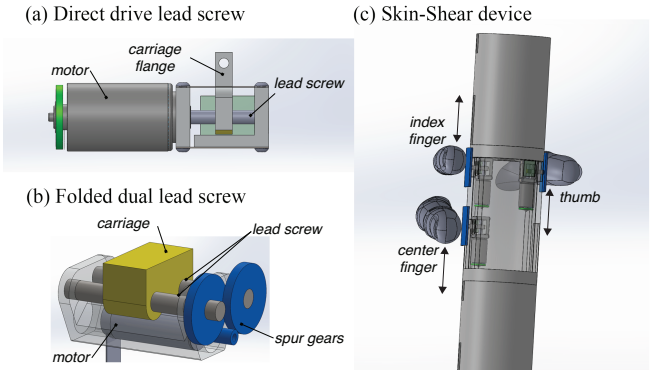

Lead screw designs, (a) direct drive and (b) dual folded drives, and their use in a handheld Skin-Shear device (c).

Skin-shear devices operate in two modes; activating different mechanoreceptor systems in each mode. In *Skin-stretch* mode, a small contactor is pre-indented in the skin and moves to activate mainly SAII fibers [12]. This mode generally requires higher forces to move the skin. Typically, skin movements of 2-5 mm are quite noticeable to users without making users uncomfortable or damaging the skin [13]. A typical human skin has lateral stiffness of 0.3-0.6 N/mm [14], therefore force requirements in this mode are in the order of 1-2 N. The second mode, *Skin-slip*, may activate other receptors depending on the texture of the contactor slipped across the skin (PC activates with rough texture and course texture activates SA1 or RA), and require low operating forces to overcome friction between the skin and the contactor. In our design, design requirements for our Skin-Shear device was set to 1-2 N force and up to 5 mm strokes at rates up to 10 cm/sec to deliver both skin-stretch and skin-slip feedback.

The organization of the paper is as follow: We first review the lead screw design and propose possible designs derived from it. We then design and fabricate an actuator assembly and presents the design analysis in Section 2. In Section 3, we present the control framework and integration of the actuator in a handheld formfactor. We then present the evaluation of

*Research supported by Facebook, Inc.
A. Israr (corresponding author) and P. Agarwal are with Facebook Reality Lab, Redmond, WA 98052 USA (e-mail: {aliisrar, pagarwal18}@fb.com).
P. Sreetharan is with Pratheev Consulting Group, MA, USA.

the actuator moving against a skin like setup and with a preliminary user study in Section 4. Finally, we conclude the paper with brief discussion and future work in Section 5.

II. Design of the Skin-Shear Actuator

A. Design Review of Lead-Screw Mechanisms

An early implementation of screws was used as pumps to lift water to higher elevations in 200 BC [15]. In recent decades, lead screws are common in high-precision motion control and are used in printers, disk drives, cameras, x-y tables, etc. This section presents a variety of design configurations derived from the lead-screw mechanism.

Direct Drive Lead Screw: Coupling the drive shaft directly to the lead screw represents the simplest and most direct way to obtain linear motion from a rotational motor (Figure 1a). The efficiency of the lead screw can be estimated using the following first-order theoretical expression [15]:

$$\eta_l = \frac{\tan(\beta)}{\tan(\beta + \arctan(f))} \qquad (1)$$

where, β is the lead angle of the screw and f is the coefficient of friction between the screw material and the coupler material connecting the screw to the carriage saddle. The efficiency can then be used to consider the relationship between the torque output by the motor (τ) and the linear output force (F) and screw lead, L:

$$F = \frac{2\pi\eta_l\tau}{L} \qquad (2)$$

Folded Lead Screws: The lead screw may also be positioned parallel to the motor and connected to the drive shaft via a pair of spur gears, as in many off-the-shelf linear actuators. For certain motor geometries, this may represent a more compact solution than directly driving a lead screw. Moreover, when the gear pair provides an additional step-down of the motor speed, it may allow the selection of a more efficient lead screw with a higher lead angle. However, this comes at the cost of design complexity, requiring more custom components and several precision alignment steps during manufacturing. Figure 1b shows a Folded Dual Lead Screw design, where the spur gears on the motor shaft simultaneously actuate two lead screws with identical gear ratios, thereby providing the anti-rotation functionality without the need for a linear bearing, reducing frictional losses and the potential for jamming.

Worm Gear and Rack: A worm gear and rack drive could, in certain cases, enable a more compact device than the lead screw configurations described above by allowing a larger fraction of the device volume to be filled up by the motor. The efficiency of a worm and rack drive is given by:

$$\eta_w = \frac{\cos\alpha_n - f\tan\beta}{\cos\alpha_n + f\cot\beta} \qquad (3)$$

where α is the normal pressure angle (typically 20° or 14.5°), β is the lead angle, and f is the coefficient of friction.

B. Motor and Design Selection

Based on the design review in previous section, we investigated off the shelf motors and computed their efficiencies (Eq. 1 and Eq. 3) and theoretical output force (Eq. 2). A subset of motors evaluated are presented in Table 1 and the efficiencies and forces are presented in Figure 2a and Figure 2b, respectively.

TABLE I. Specification of Off-the-Shelf Motors

Vendor	*PN*	*Type*	*Dia (mm)*	*Length (mm)*	*Torque[a] (mNm)*	*Speed[b] (rpm)*	*Lead[c] (mm)*
Precis. Micro.	106-002	Brushed	6	12.2	0.05	14000	0.429
Precis. Micro.	107-001	Brushed	7	16.6	0.09	4320	1.389
Precis. Micro.	108-106	Brushed	8×6	14.5	0.15	12600	0.476
Micromo	0615 S	Brushed	6	15.3	0.17	2500	2.400
Micromo	0816 S	Brushed	8	19.5	0.15	13000	0.462
Micromo	AM 0820	Stepper	8	16.75	0.34	18000	0.333

a. Maximum rated output force as specified in the datasheet.
b. Maximum rated speed as specified in the datasheet.
c. Linear lead per revolution of motor shaft for 10 cm/s linear output speed at max. motor speed.

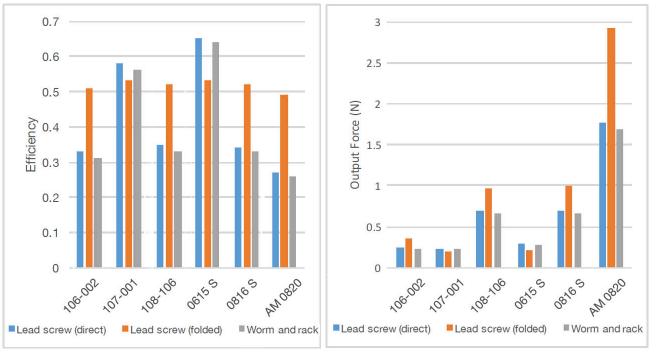

Figure 2. Efficiency and theoretical force output of available motors.

The blue bars in Figure 2 show theoretical direct drive lead screw efficiencies and projected output forces for the motors listed in Table 1. It is assumed that the lead is equal to the values given in Table 1; in practice, the exact lead may not be available. The output force calculation does not consider the losses associated with the anti-rotation mechanism of the lead screw, and the theoretical expressions tend to overestimate efficiency (and consequently, output force).

The orange bars in Figure 2 represent calculations for a folded lead screw design, with an additional 1:5 or 1:2 step-down in the gearing mechanism (selected to maximize efficiency). Despite mechanical losses in the spur gears, the increase in lead screw efficiency generally results in higher output forces for motors with higher rated speed. However, this comes at the cost of design complexity.

The gray bars in Figure 2 show efficiency and force calculations for a worm and rack design. Efficiency values tend to be similar (if slightly lower) than a comparable direct-drive lead screw. However, the worm gear and rack drive involve several important drawbacks vs. lead screw configurations: less surface area for carrying the load (and therefore increased wear), an asymmetric axial load on the motor shaft, and the requirement of a specialized linear bearing for the rack. The linear bearing would be significantly more complicated to design than a lead screw anti-rotation mechanism, potentially more prone to jamming, and would likely incur more frictional losses, reducing output force.

Based on design considerations, component availability and simplicity, we proceeded with the direct drive lead-screw design using AM0820 stepper motor (Micromo, FL, USA).

C. Mechanism Design

We chose the direct drive lead screw configuration due to its simple configuration. The major challenges are enduring forces and torques back-driven from the output and ensuring frictional forces from the required anti-rotation bearing are contained. Most notably, the mechanism must survive forces applied, most notably a nominal 10 N normal force caused by a user pressing the moving assembly from above. For rapid prototyping, we used AM0820 stepper motor. The motor has integrated lead screw and nut options from the manufacturer, eliminating assembly risk, and the performance of lead screw and nut are well characterized, therefore, eliminating much of the guesswork. Moreover, the motor comes with an internal shaft bearing with rated force of 3 N. Figure 3 shows components of designed actuator assembly.

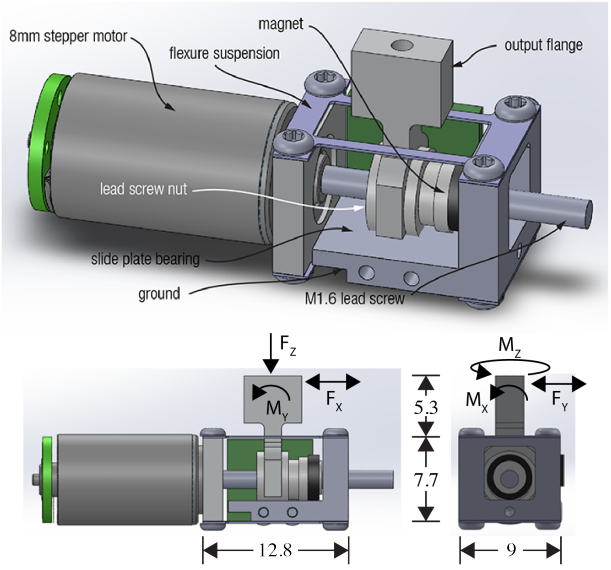

Figure 3. Design of the actuator assembly using direct drive lead screw. All dimensions are in millimeters.

The motor assembly plate is attached to the ground plate using a dual flexural spring at the top and bottom. An output flange is designed to press-fit to the nut and has a threaded hole on the top to screw in skin contactors. To prevent rotation of the nut on the lead screw, we have opted for a slide plate bearing formed by a flat region of the nut and a polished aluminum surface on the ground plate. This strategy is the simplest to implement and enables us to take advantage of the engineered bearing plastic already in use for the lead screw nut. The anti-rotation bearing has a small nominal gap between bearing surfaces. The dual flexure spring between ground and motor assembly maintains this gap and lead screw orientation while providing compliance in the normal direction. An excessive normal force flexes the spring, closing the gap and jamming the output nut against ground. Any force above that needed to close the gap is not transmitted to the motor. The nut is a proprietary formulation of self-lubricating PEEK whose frictional coefficients is approximated to be 0.1.

Accurate position sensing is challenging in a small form factor. We attempt to accommodate a linear hall effect sensor. An eccentric magnet (appears black in Figure 3) is mounted on the motor shaft, with magnetic axis aligned with the axis of the motor shaft. Figure 4d shows two readings of the hall effect sensor along three axes taken a day apart.

D. Design Analysis

The overall actuator is 25 mm long, 8 mm in height and 9 mm wide. The carriage (flange) assembly moves 6 mm, in both directions, along the axis of the lead screw and weighs 5 grams. Since the rated force of the motor is low (~ 1.5 N), it is critical to investigate performance of the design under load. Assume a 10 N applied force with 1 N required to close the bearing gap. The remaining 9 N is applied to the slide plate over an area of approximately 6 mm^2 for a pressure of 1.5 MPa (218 psi). This means there will be a 0.9 N frictional force opposing the motion of the output. Referring to the expected output force (Figure 2), the mechanism is expected to survive the specified 10 N applied force and continue to operate.

There are six independent forces and torques that a user can apply to the output carriage of the lead-screw. They are:

Normal force, F_z: The user pressing down is protected as previously described. Pulling upwards is vulnerable, but unlikely to be experienced. Upwards can be protected by an additional jamming surface above the nut.

Transverse force, F_y: Protected by interference between mechanism output and slot in the housing structure.

Longitudinal force, F_x: Vulnerable. The solution is to add thrust bearings onto the lead screw. The back drivability of the lead screw requires significant forces at the carriage, and therefore this is not currently implemented.

Torque about normal, M_z: Vulnerable. The solution is to use a compliant finger pad or dual bearings on the lead screw, the latter of which is not implemented.

Torque about transverse, M_y: Protected by normal force protection, because this torque is very difficult to generate without accompanying normal force.

Torque about longitudinal, M_x: Protected by interference between mechanism output and slot in the housing.

In this first implementation, the motor is protected from the most important applied forces and torques. Solutions for protecting the device from the remaining forces and torques in are remained for future designs.

III. Integration and Controls

A. Electronic Components

We used the A4988 integrated circuit (Allegro Microsystems, NH USA) as the driver for each individual stepper motor. The A4988 features a simple STEP/DIR interface, and is capable of micro-stepping down to 16 steps per individual motor step. We anticipate using two-phase full-step mode to maximize torque, as the motor and lead screw configuration is 80 steps per 1 mm of linear motion, and cogging is not expected to be discernible by users, however, micro-stepping can be utilized if cogging becomes a concern.

We selected the MLX90365 3-axis Hall effect sensor from Infineon to implement position sensing. The sensor is available in a compact SOT 23-6 package that fits on the miniature PCB (green plate shown in Figure 3) without adding substantially to the overall device dimensions. The Teensy 3.2

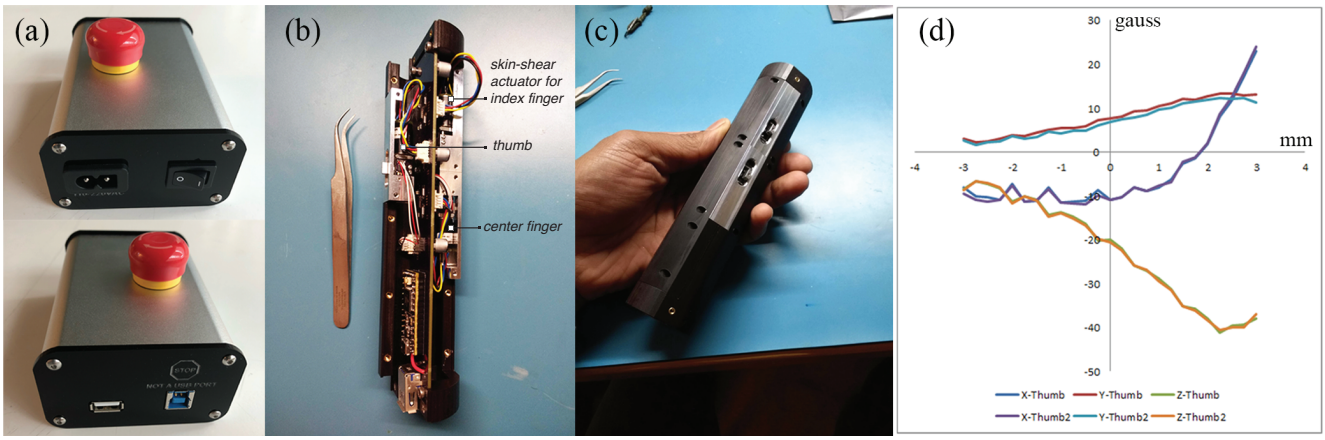

Figure 4. (a) Front and back views of power enclosure. (b) Open view and (c) close view of the handheld prototype. (d) Two readings (takens one day apart) of three axes of Hall Effect sensor (in gauss) and travelled distance (in mm).

USB development board, powered by a Cortex-M4 processor, will serve as the master controller, interfacing directly with the A4988 drivers via two I/O pins each and the MLX90365 Hall effect sensors via I2C interface.

An external power enclosure (Figure 4a) provides 18V power to the motor drivers, and also serves as a USB 2.0 pass-through to establish a connection between a host computer and the Teensy controller. Both the motor drivers and the Teensy are located on the main control board, placed inside the prototype (Figure 4b). The enclosure features an on/off switch as well as a top-mounted emergency stop button to interrupt power to the motors without de-powering the Teensy controller.

B. Software Interface

A Teensy 3.2 runs the prototype on an Arduino software stack (www.arduino.cc). Communication between the prototype and the host computer is conducted over a serial port using the `CmdMessenger` library, which is available as standard on the Arduino Platform. A user interface is developed as a python application that can be installed using the python3 pip interface and relies on the pyCmdMessenger implementation of the library (Figure 5). The software implements a generic API to communicate between the computer and Teensy and six general classes of haptic effects are shown in the user interface. Users can vary parameters of the shear, such as shear displacement, shear rate, frequency of oscillation, and the maximum force factor, using control widgets on the interface. The six classes are:

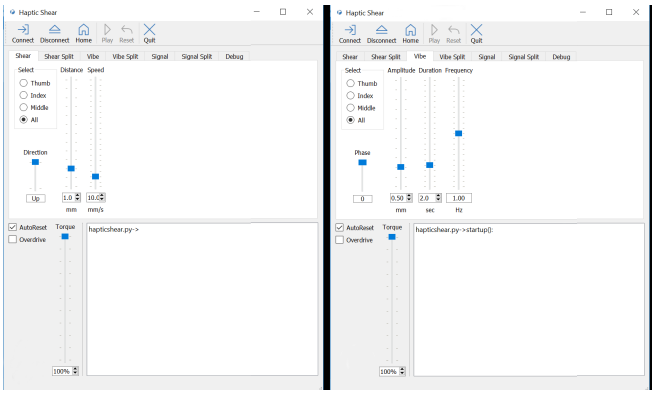

Figure 5. Graphical user interface for (a) shear stroke profiles and (b) sinusoidal profiles.

1) Single finger shear effects

2) Multi-finger independently parametrized shear effects

3) Single finger vibration effects

4) Multi-finger independently parametrized vibrations

5) Single finger arbitrary custom waveform effects

6) Multi-finger arbitrary custom waveform effects

We run the stepper motors in open-loop control, side-stepping the use of Hall effect sensor readings for closed-loop control, where commanded displacements are converted into number of steps for the motors to move per unit time frame. The update loop in the Teensy was set to 5 kHz, while the USB communication was set at 115200 baud rate.

B. Handheld Prototype

We realized a handheld prototype that houses three actuators in a configuration that allows a simple grasp to interface index finger, middle finger, and thumb with the actuators, as shown in Figure 4c. The majority of the prototype is 3D-printed with slots cut for the carriage assembly of each actuator to protrude outward. Machined brackets have been introduced at each actuator, since the precision of 3D printing is insufficient to directly mount the miniaturized actuators.

The prototype body also houses the main control board, to which Teensy and motor drivers are attached (Figure 4b), to simplify cabling requirements and to enable use of a stock cable from the prototype to bench-top power enclosure. The prototype is designed to have replaceable finger pads as well as mounting points to affix grounded structures to the prototype's body. The prototype is made flat along its axis to accommodate grounding strips to support and resist the fingers to exert high axial forces, at the same time maintaining a consistent contact between the fingers and the carriage.

Several finger pad designs were printed and tested for comfort and efficiency of the system. We varied material of the pads, their size, their finish and texture, and height of the pad indented into the skin. Based on preliminary assessments, we selected pads with stiffer material (3D printed acrylonitrile

styrene acrylate), having textured surface (hemispherical dots of radius 0.25 mm per mm^2 uniformly distributed on the finger pad surface) orthogonal to the direction of motion every 0.5 mm) and size (12.7 mm × 4.5 mm), and is slightly recessed below the height of the grounding strip, however, further evaluation is left for future user studies to determine best coupling for skin-shear devices.

IV. Experimental Evaluations

The evaluation of the actuator is done in two ways. One, we measure mechanical behavior of the actuator in the free condition and when loaded with a spring to mimic skin dynamics and plot the displacement of the carriage to highlight possible mismatches between the applied (open-loop) and measured displacements. Two, we conduct a preliminary user study to determine throughput (in terms of information transfer) of the 3-digit prototype and determine possible causes of perceptual confusions. A formal user study to characterize skin-shear and its use to enhance virtual reality experiences is left for future.

A. Mechanical Characterization

Mechanical characterization of a single actuator is performed by clamping the prototype to a vibration isolation table and moving the carriage to set locations by predefined step values for the motor. Figure 6a shows a set up for the test. In *unloaded* conditions, displacement of the saddle is measured using a laser vibrometer and compared against command inputs to the motor. In the *loaded* configuration, an adapter of known spring loading barely rests against the saddle and command inputs are repeated. The stiffness of the spring (k) is 359 N/mm, roughly matching with the stiffness of the skin in stretching and lateral deformations (300 N/m–500 N/m [14]). This is to ensure that the actuator will reliably move and laterally deform the skin.

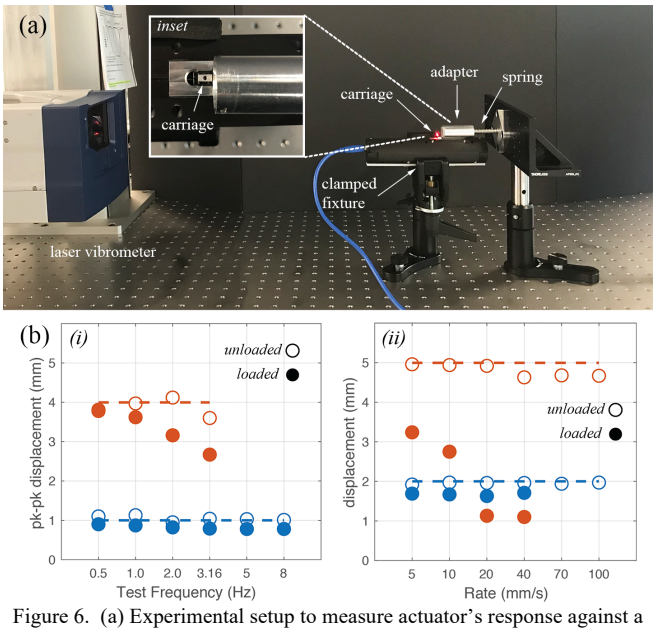

Figure 6. (a) Experimental setup to measure actuator's response against a load of known stiffness. (b) Displacement of the carriage saddle as a function of frequencies (i) and as rate of linear motion (ii). Dashed lines are refernce command inputs.

Two type of profiles are tested. In *sinusoidal* profiles, the saddle is commanded to move with a sinusoidal motion of test frequencies (0.5, 1, 2, 3.16, 5 and 8 Hz) and with two peak-to peak-amplitudes (1 mm and 4 mm). The duration of stimulation was set to 8 seconds to ensure capturing multiple cycles. In *ramp* profiles, the saddle is commanded to move with strokes of 2 mm and 5 mm at six stroke rates (5, 10, 20, 40, 70 and 100 mm/second), repeated thrice. Figure 6b shows loaded and unloaded response of the actuator with sinusoidal (panel (i)) and ramp (panel (ii)) profiles. Open-loop command inputs (shown as dashed lines) matches with movements of the carriage saddle in unloaded conditions (open symbols), specifically at low amplitude movements. At high amplitudes, the actuator suffers due to bandwidth and seize to operate beyond 4 Hz. At lower amplitudes, 0.5 mm and below, the actuator's movement was perceivable beyond 15 Hz.

Loaded responses (filled symbols) show deterioration in actuator performance, specifically at high strokes, and further deteriorates with increasing frequency and stroke rate. This could be due to the software limit to restrict sudden changes in motor acceleration which may cause skipping steps and motor damage, and due to the open-loop stepper control scheme. Nevertheless, at low rates, the carriage saddle deforms the impeding spring greater than 3 mm, thereby achieving the output force greater than 1 N.

B. Preliminary Perceptual Analysis

A pilot study is conducted to evaluate the effective of skin shear for communication through three digits of the human hand (Figure 1c), and to determine possible confusions between digits. In comparison, the same test is performed with three vibrotactile actuators placed on same three digits. Two coauthors participated in the pilot session of ~30 minute and held the prototype between three fingers as shown in Figure 7. The session was divided into two blocks, one participant completed the skin-shear block first and then the vibrotactile block and the other participant was tested in the reverse order. They were tested in absolute identification tasks and asked to identify the location or locations of haptic stimulation. Haptic stimulation was played through three digits (1: thumb, 2: index finger, and 3: center finger) with seven possible combinations of single- or multi-digit activation. Each block had 105 trials, i.e. 15 repetitions of seven stimuli, presented in a randomized order. No correct answer feedback was provided in both blocks. Details of the procedures and analysis of data was same as in [16].

In the skin-shear test, a ramp profile (stroke: 5 mm, and rate: 10 mm/s, duration: 0.5 seconds) was simultaneously rendered through one or multiple actuators. Participants responded with a number between 1 and 7 corresponding to seven outcomes ([1], [2], [3], [1,2], [1,3], [2,3], [1,2,3]), which were graphically illustrated in a handout placed in front of them. In the vibrotactile test, three small LRAs (model: 1040, Mplus Co., S. Korea) are placed on the same locations on the 3D casing and vibrated with 160 Hz sinusoid at roughly 30 dB SL. Vibration duration was set to 0.5 seconds with 50 milliseconds of ramp-up and ramp-down. Participants responded with a number 1-7 corresponding to the locations of vibration source. Both participants wore noise cancellation head phones during the study and were asked not to see the handheld prototype.

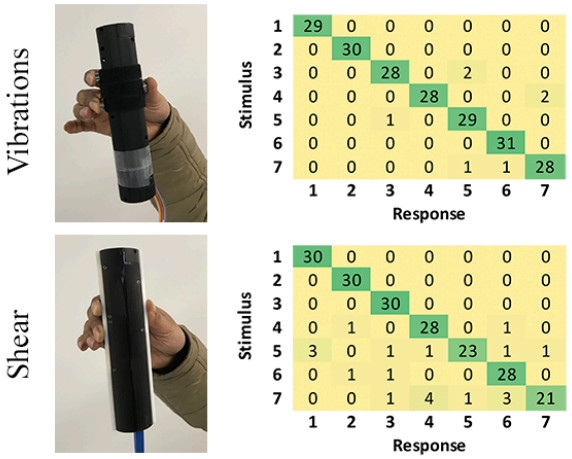

Figure 7. Holding postures of vibrational (top) and skin-shear (bottom) prototypes and corresponding stimulus-response confusion matrices.

Stimulus-response matrices for both types of haptic cues are shown in Figure 7. In both cases, the identification performance of seven stimulus was close to perfect, however, vibration modality yielded slight better performance accuracy (PC=96.7%, IT=2.62 bits) than the shear modality (PC=90.5, IT=2.3 bits). In the shear mode, most confusion occurred when all three digits were simultaneously occurred, indicating higher spatial masking with the shear cues. In the vibration mode, simultaneous activation of three digits increased the overall perceived intensity of vibrations, which might have given participants indication of all three digits.

V. Concluding Remarks and Future Directions

In this paper, we present and evaluate a design of Skin-shear actuator, based on the lead screw mechanism. Our design is simple, consists of small number of components, accommodates in a compact and light form factor for handheld and wearable embodiments, and offers forces and displacements sufficient for skin-stretch and skin-slip applications. Such actuators can be integrated into hand controllers, cell phone devices, sun glasses and head mounted gears, shoes and wristband to enhance user interactions during playing games, watching movies, AR and VR applications. We have integrated three of such actuators in a handheld prototype to render shear cues on three digits of a hand. An initial user study shows that the information throughput at three digits is comparable to that of vibrations. We will further evaluate the use of Skin-shear actuators during dynamic interactions with virtual objects and study sensory illusions it elicits by synchronously and asynchronously activating individual channels. For example, simultaneous activation of multiple digits gives sensory illusion of pull and push forces, and sequential onsets induces illusions of locomotion. Such illusions will be studied in full extend in the future.

We used the lead screw with a stepper motor, mainly due to availability of components and adequate documentation, and reduction in complexity. They have some drawbacks for acting as skin-shear devices, most notably, the rated torques for stepper motors are generally lower than dc motors of the same size, stepper control is complicated than DAC voltage control for dc motors, motion of the carriage saddle is limited to discrete levels which can induce vibrations, and rendered force are not continuous, therefore limiting the performance of the lead screw design presented here. In the future, we will replace the motor with an alternate option, such as with a dc or piezo-based motors and compare performance in other smaller form factor devices. In addition, the performance of the device can be further improved by utilizing the position measurements in a closed-loop force or displacement control scheme and will be further explored in the future.

Acknowledgment

This work is supported by Facebook, Inc.

References

[1] S. Choi and K. J. Kuchenbecker, "Vibrotactile display: Perception, technology, and applications, *Proceedings of the IEEE*, vol. 101, no. 9, pp.2093-2104, 2013.

[2] A. Girard, M. Marchal, F. Gosselin, A. Chabrier, F. Louveau, and A. Lécuyer, "Haptip: Displaying haptic shear forces at the fingertips for multi-finger interaction in virtual environments," *Frontiers in ICT*, vol. 3, no. 6, 2016.

[3] S. B. Schorr and A. M. Okamura, "Fingertip tactile devices for virtual object manipulation and exploration," in *Proceedings of the 2017 CHI Conf. on Human Factors in Computing Systems*, pp. 3115-3119, 2017.

[4] E. Pezent, A. Israr, M. Samad, S. Robinson, P. Agarwal, H. Benko, and N. Colonnese, "Tasbi: Multisensory squeeze and vibrotactile wrist haptics for augmented and virtual reality," in *Proceedings of the IEEE World Haptics Conference,* 2019, submitted for publication.

[5] S. Gupta, T. Campbell, J.R. Hightower, and S. N. Patel, "SqueezeBlock: using virtual springs in mobile devices for eyes-free interaction," in *Proceedings of the 23nd Annual ACM Symposium on User Interface Software and Technology*, 2010, pp. 101-104.

[6] F. Chinello, C. Pacchierotti, J. Bimbo, N. G. Tsagarakis, and D. Prattichizzo, "Design and evaluation of a wearable skin stretch device for haptic guidance," *IEEE Robotics and Automation Letters*, vol. 3, no. 1, pp. 524-531. 2018.

[7] K. Bark, J. Wheeler, G. Lee, J. Savall, and M. Cutkosky, "A wearable skin stretch device for haptic feedback," in *IEEE World Haptics Conference*, 2009, pp. 464-469.

[8] N. G. Tsagarakis, D. G. Caldwell, and T. Horne, "Slip Aestheasis: A portable 2d slip/skin stretch display for the fingertip, in *IEEE World Haptics Conference*, 2005, pp. 214-219.

[9] R. J. Webster, T. E. Murphy, L. N. Verner, and A. M. Okamura, "A novel two-dimensional tactile slip display: design, kinematics and perceptual experiments," *ACM Transactions on Applied Perception*, vol. 2, no. 2, pp. 150-165, 2005.

[10] N. I. Berg, R. K. Holm, and P. O. Rasmussen, "Theoretical and experimental loss and efficiency studies of a magnetic lead screw," in *Energy Conversion Congress and Exposition*, pp. 2185-2192.

[11] C. C. Wei and R. S. Lai, "Kinematical analyses and transmission efficiency of a preloaded ball screw operating at high rotational speeds," *Mechanism and Machine Theory*, vol. 46, pp.880-898, 2011.

[12] D. Purves, G. J. Augustine, D. Fitzpatrick, et al., "Mechanoreceptors Specialized to Receive Tactile Information," *Neuroscience*, 2nd edition, 2001. Available from: https://www.ncbi.nlm.nih.gov/books/NBK10895/

[13] B. T. Gleeson, S. K. Horschel, and W. R. Provancher, "Perception of direction for applied tangential skin displacement: Effects of speed, displacement, and repetition," *IEEE transactions on haptics*, vol. 3, no. 3, pp.177-188, 2010.

[14] N. Nakazawa, R. Ikeura, and H. Inooka, "Characteristics of human fingertips in the shearing direction," *Biological cybernetics*, vol. 82, no. 3, pp. 207-214, 2000.

[15] A. Slocum, "Topic 6: Power Transmission Elements II," in *FUNdaMENTALS of Design*. 2008. Available from: http://pergatory.mit.edu/resources/FUNdaMENTALS.html.

[16] H. Z. Tan, N. I. Durlach, C. M. Reed, and W. M. Rabinowitz, "Information Transmission with a multifinger tactual display," *Perception & Psychophysics*, vol. 61, no. 6, pp. 993-1008, 1999.